High Power Laser Science and Engineering, (2025), Vol. 13, e15, 11 pages.
doi:10.1017/hpl.2024.91

HIGH POWER LASER SCIENCE AND ENGINEERING

RESEARCH ARTICLE

High-fidelity delivery of kilowatt-level single-mode lasers through a tapered multimode fiber over one hundred meters

Xiao Chen[1,†], Shanmin Huang[1,†], Liangjin Huang[1,2,3], Zhiping Yan[1,2,3], Zhiyong Pan[1,2,3], Zongfu Jiang[1,2,3], and Pu Zhou[1]

[1]*College of Advanced Interdisciplinary Studies, National University of Defense Technology, Changsha, China*

[2]*Nanhu Laser Laboratory, National University of Defense Technology, Changsha, China*

[3]*Hunan Provincial Key Laboratory of High Energy Laser Technology, National University of Defense Technology, Changsha, China*

(Received 6 July 2024; revised 16 November 2024; accepted 2 December 2024)

Abstract

The immediate priorities for high-power delivery employing solid-core fibers are balancing the nonlinear effect and beam deterioration. Here, the scheme of tapered multimode fiber is experimentally realized. The tapered multimode fiber, featuring a 15 m (24/200 μm)–10 m (tapered region)–80 m (48/400 μm) profile, guides the laser with a weakly coupled condition. With the input power of 1035 W, the maximum output power over the 105 m delivery is 962 W, corresponding to a high efficiency of over 93% and a nonlinear suppression ratio of over 50 dB. Mode resolving results show high-order-mode contents of less than –30 dB in the whole delivery path, resulting in a high-fidelity delivery with M^2 factors of 1.20 and 1.23 for the input and output lasers, respectively. Furthermore, the ultimate limits of delivery lengths for solid-core weakly coupled fibers are discussed. This work provides a valuable reference to reconsider the future boom of high-power laser delivery based on solid-core fibers.

Keywords: hundred meters; laser delivery; nonlinear effect; single mode; tapered multimode fiber

1. Introduction

High-power single-mode laser delivery has become a renewed interest recently[1–4], due to its potential applications in extreme manufacturing, precise welding and the defense industry[5]. Solid-core delivery fibers offer a brilliant solution for high-power delivery, and this success is driven by the integrated compact for flexible operation and robust laser confinement. At present, many scenarios spawn a compound demand for high-power, single-mode and long-distance delivery; for instance, the application of precise welding needs a single-mode beam to promote working efficiency and simultaneously a long-distance delivery to expand the processing range.

The existing solid-core fiber-based laser delivery system has a technical bottleneck in that the power, beam quality and nonlinear threshold cannot be balanced. For single-mode lasers operating at several kilowatts, the main obstacles impeding long-distance delivery are nonlinear effects and beam quality degradation. For industrial fiber lasers with a broadband spectrum, the dominant nonlinear effect is stimulated Raman scattering (SRS)[6,7]. To increase the delivery distance, extended-mode-area (EMA) fibers with enhanced nonlinear thresholds are needed. However, multimode operation in the large core diameter accelerates the degradation of beam quality in the whole delivery path. Although the research in single-mode laser sources has pushed the power record to the order of several kilowatts[8] and even 10 kW[9], the results with a long-distance single-mode delivery over more than tens of meters[4,10] are far behind, which severely limits the performance of laser beams reaching the workbench. To handle this bottleneck, the key is seeking a bilateral solution for preserving high-fidelity transmission and improving the nonlinear threshold.

An effective strategy is developing special fibers with increased high-order-mode (HOM) losses, which has led to multiple fiber designs[11–13], including modified clad profiles or microstructure fibers. A variety of designs, such as single-trench fiber[14,15], chirally coupled-core fiber[16] and all-solid photonic bandgap fiber[17], have seen stages of success in surpassing conventional fibers. A higher HOM loss extends the possibility of enlarging the core diameter,

Correspondence to: L. Huang, Z. Pan and P. Zhou, College of Advanced Interdisciplinary Studies, National University of Defense Technology, Changsha 410073, China. Emails: huangliangjin203@163.com (L. Huang); panzy168@163.com (Z. Pan); zhoupu203@163.com (P . Zhou)
[†]These authors contributed equally to this work.

yielding a robust single-mode operation and a higher power scalability. However, it is a general fact that these special fibers suffer from more complex preparation processes, more stringent manufacturing tolerances and limited practicality for integration. Owing to the greater bending sensitivity, the future boom for them is more likely to obtain gain fibers with moderate lengths rather than long-distance delivery fibers. Hence, more efforts should be afforded to facilitate their applications, especially compact integrations with conventional fibers[18]. Recent research has demonstrated the integration potential of a solid-core microstructure fiber with a conventional fiber, which enables a 10 kW laser delivery of over 30 m[19].

Recently, hollow-core fiber (HCF) has become a rising star in the field of single-mode and long-distance delivery[1,3,20,21]. HCFs offer the unprecedented advantages of low nonlinearity, an excellent single-mode property and a high damage threshold, which makes them a highly attractive option for the long-distance delivery of high-brightness laser beams. Moreover, the loss record of HCFs has refreshed rapidly in recent years, and the latest records achieved by HCFs present comparable loss values to those of conventional fibers covering broadband spectrum regions[22,23]. Up to now, the record-breaking delivery length has been confirmed in multiple wavebands, ranging from the conventional 1 μm waveband (1000 m)[1] to the mid-infrared (108 m)[24] and visible (300 m)[25] regions. These results simultaneously validate the power handling capacity of HCFs above kilowatts for both continuous and pulsed laser regimes. HCFs create an air-based environment to facilitate the nonlinear-effect-free delivery of high-power lasers, and future attempts should be focused on realizing compact and highly efficient integrations with the current laser systems. However, all of the high-power delivery results have been achieved based on spatially coupled architectures currently, which suffer from thermally induced focusing shifts at different power levels. Hence, the stability is limited, and discontinuous adjustments are required during the power scaling process.

Another strategy is controlling the mode coupling in conventional fibers while enlarging the core diameters, which gives rise to the weakly coupled fiber[26]. With the weakly coupled condition, fiber modes propagate along the long-distance path with high fidelity, and the adjacent modes have negligible mode coupling coefficients. The mode coupling between the fundamental mode and the HOMs obeys the field coupling equation, in which the phase matching condition is strongly correlated to the propagation constant (β) difference. In other words, a weakly coupled condition, represented by a large β difference, means a large index difference Δn_{eff} between adjacent modes. Therefore, the high-fidelity delivery of conventional fiber should consider a tradeoff between the maximum core diameter and the numerical aperture (NA)[4]. The investigations of weakly coupled fiber date back to 1998, in which Fermann[27] reported the preservation of the fundamental mode with a core diameter of 45 μm and emphasized the beneficial effect of a larger cladding diameter. Since then, high beam quality outputs have been experimentally demonstrated in 100–400 μm core diameters[28,29]. The remarkable advances in 2014 and 2019 showed great examples in balancing the core diameter and NA for weakly coupled delivery, resulting in an 800 W, 100 m delivery in the 30 μm fiber and a 1000 W, 100 m delivery in the 60 μm fiber. In these investigations, a key procedure is the dominated excitation of the fundamental mode, for example, employing a cascade mode field adapter[4]. However, as a type of fiber device, the mode field adapter has limited power handling ability and suffers from inescapable mode degradation due to intrinsic defects during fabrication[30,31].

The immediate priorities are looking for solutions for the two key issues: (1) how to improve the nonlinear threshold of long-distance delivery and (2) how to achieve high-fidelity delivery by optimizing the launching condition and preventing transmission deterioration. In this work, the solution of tapered multimode fiber is proposed. We attempt to push the delivery of kilowatt-level, single-mode lasers to over 100 m based on a monolithic, solid-core, weakly coupled and tapered multimode fiber, featuring a high-fidelity delivery without beam quality deterioration. In Section 2, the design principle of the multimode tapered fiber and the fabrication results are presented. In Section 3, the high-fidelity delivery of a kilowatt-level single-mode laser is experimentally demonstrated. The results show a high transmission efficiency of over 93%, a high signal-to-SRS ratio of over 50 dB and a high-fidelity delivery with negligible beam degradation. In Section 4, the ultimate limits of delivery length for the single-mode laser with different powers are discussed for reference.

2. Weakly coupled fiber and fiber fabrication

The high-fidelity transmission of a single-mode laser means that the fundamental mode remains isolated from the HOMs, preventing possible energy exchange between them. In an ideal multimode fiber, the eigenmodes are intrinsically orthogonal and propagate through independent channels. Nevertheless, unexpected perturbations within actual fibers, such as slight fluctuations in the refractive index or geometric dimensions, and bending distortion, can impact the mode isolation. In this way, owing to the uniform perturbation of the local dielectric constant, the fundamental mode and the HOMs are easily coupled to each other over a long-distance delivery. The strength of mode coupling between modes is determined by the phase matching condition, which is related to the propagation constant difference of modes. Generally, the strength of mode coupling between adjacent modes is dominant, and a larger mode spacing results in a decreased mode coupling. Hence, the key issue for the high-fidelity delivery of single-mode lasers is increasing the mode

spacing between the fundamental mode and the LP_{11} mode. The coupled mode equations for the two modes are written as follows[32]:

$$\begin{cases} \frac{dA_1}{dz} = iK_{11}A_1 + iK_{12}A_2 \exp[i(\beta_2 - \beta_1)z], \\ \frac{dA_2}{dz} = iK_{22}A_2 + iK_{21}A_1 \exp[i(\beta_1 - \beta_2)z], \end{cases} \quad (1)$$

where A_1 and A_2 are the amplitudes of two modes, β_1 and β_2 are the propagation constants of two modes and the coupling efficiencies K_{12} and K_{21} obey the symmetry relation $K_{12} = K_{21}$.

According to the coupled mode equations, a phase matching condition should be fulfilled to allow sufficient mode coupling. This means that the strength of mode coupling could be reduced by enlarging the propagation constant difference $\Delta\beta$ or effective index difference Δn_{eff} between modes. Therefore, one can conclude that it might be appropriate to employ weakly coupled multimode fibers with a high effective index difference instead of single-mode fibers to transport a single-mode beam. From the birefringence of commercially available polarization-maintaining fibers, it can be deduced that the polarization mode coupling is efficiently suppressed when the effective index difference Δn_{eff} between adjacent modes is larger than 5×10^{-4}. Furthermore, Fini[33] and Fini and Ramachandran[34] stated that the reference value to meet the weakly coupled condition could be limited to the target as follows:

$$\Delta n_{\text{eff}} > 1 \times 10^{-4}. \quad (2)$$

To achieve the weakly coupled condition, both a large refractive index contrast between the core and the cladding and a small core diameter are needed[35]. However, a small core diameter reduces the effective mode area, which accelerates the nonlinearities for long-distance delivery. Here, a tradeoff among the core diameter, NA and Δn_{eff} between the fundamental mode and the LP_{11} mode is calculated. According to the results in Figure 1(a), the Δn_{eff} shows an inverse proportional relationship with the core diameter. A higher value of NA induces a larger Δn_{eff}, corresponding to a better weakly coupled condition. However, for core diameters above 40 μm, the Δn_{eff} and NA have less correlation for a fixed core diameter. This phenomenon restricts further scaling of the core diameter to satisfy the weakly coupled condition even with a large NA value. Based on the principle defined in Equation (2), the maximum core diameter obeying the weakly coupled condition is confined to around 50–60 μm. This principle will guide the design of the tapered multimode fiber drawn in this work.

Subsequently, the tapered multimode fiber is drawn adiabatically by using the fiber drawing tower, and the measured fiber dimension profile along the longitudinal direction is as plotted in Figure 1(b). As shown in Figure 2(a), the core/clad dimensions at the thin and thick ends are nearly 24/200 and 48/400 μm, respectively. The effective mode areas at the thin and thick ends are calculated to be 347 and 1089 μm^2, respectively. The total fiber length is 105 m, comprising a thick region of 80 m, a tapered region of 10 m and a thin region of 15 m. The measured refractive index profile is shown in Figure 2(b), and the NA is approximately 0.06. The cut-back test indicates a core attenuation of approximately 3.5 dB/km at the signal wavelength (1080 nm), which guarantees a relatively high efficiency (>90%) for the delivery application of over 100 m.

The profile of the tapered fiber is designed by considering the balance among the weakly coupled condition, mode matching with the laser source and the nonlinear suppression. At the thin end, the mode matching between the tapered fiber and the output fiber of the laser source should be considered. The core/cladding ratio of the tapered fiber results in a few possible specifications for the thin end, for example, 20/167, 24/200 or 30/250 μm. The output fiber of the laser source has the dimension of 20/250 μm. Hence, compared with 30/250 μm, the dimension of 24/200 μm is more favorable to achieve mode matching with the output fiber of the laser source. To prevent mode degradation over a long delivery path, the maximum core diameter at the thick end should obey the weakly coupled condition. Based on the principle defined by $\Delta n_{\text{eff}} > 1\times10^{-4}$, the maximum core diameter obeying the weakly coupled condition is confined to around 50–60 μm. For a moderate and secure consideration, the core diameter at the thick end is limited to below 50 μm, which is a moderate value to realize a large mode area and high-fidelity transmission. Therefore, based on these considerations, the profiles of 24/200 and 48/400 μm are selected finally.

Through the repeat fiber drawing experiments, the optimized interval from nearly 8 to 12 m for achieving a uniformly shrinkable taper is found. Hence, a moderate length of 10 m for the tapered region is selected for achieving a uniformly shrinkable taper (from 48/400 to 24/200 μm), which is vital for mode preservation. To enhance the nonlinear threshold, the thick end should dominate the entire length of the tapered delivery fiber. In addition, to reach the goal of high-power laser delivery over 100 m, the total length of the thin and thick ends should be longer than 90 m (considering the taper length of 10 m). Hence, the ultimate design determines the respective lengths of the thin and thick ends. There are a few optional schemes, for instance, (i) 5 m (thin end) and 90 m (thick end), (ii) 10 m (thin end) and 85 m (thick end), (iii) 15 m (thin end) and 80 m (thick end). It is a clear fact that the effective mode area of the tapered fiber increases gradually from scheme (i) to (iii), which means stronger SRS suppression. Therefore, if scheme (iii) can realize a high-quality (signal-to-SRS ratio of over 50 dB) delivery over 100 m, schemes (i) and (ii) will undoubtedly be even better.

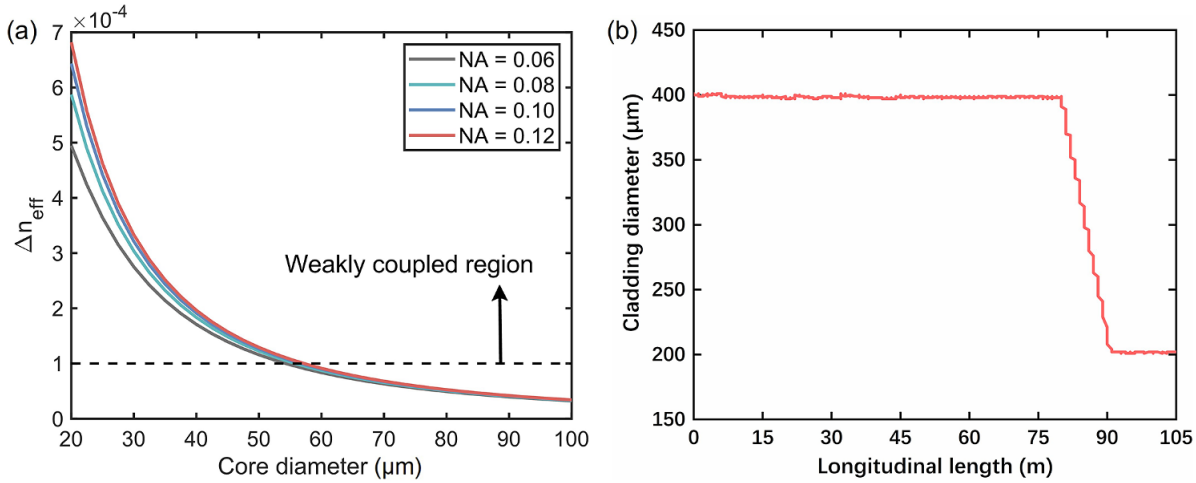

Figure 1. (a) Calculated results of effective index differences with different fiber parameters. (b) Measured fiber dimension profile of the tapered multimode fiber.

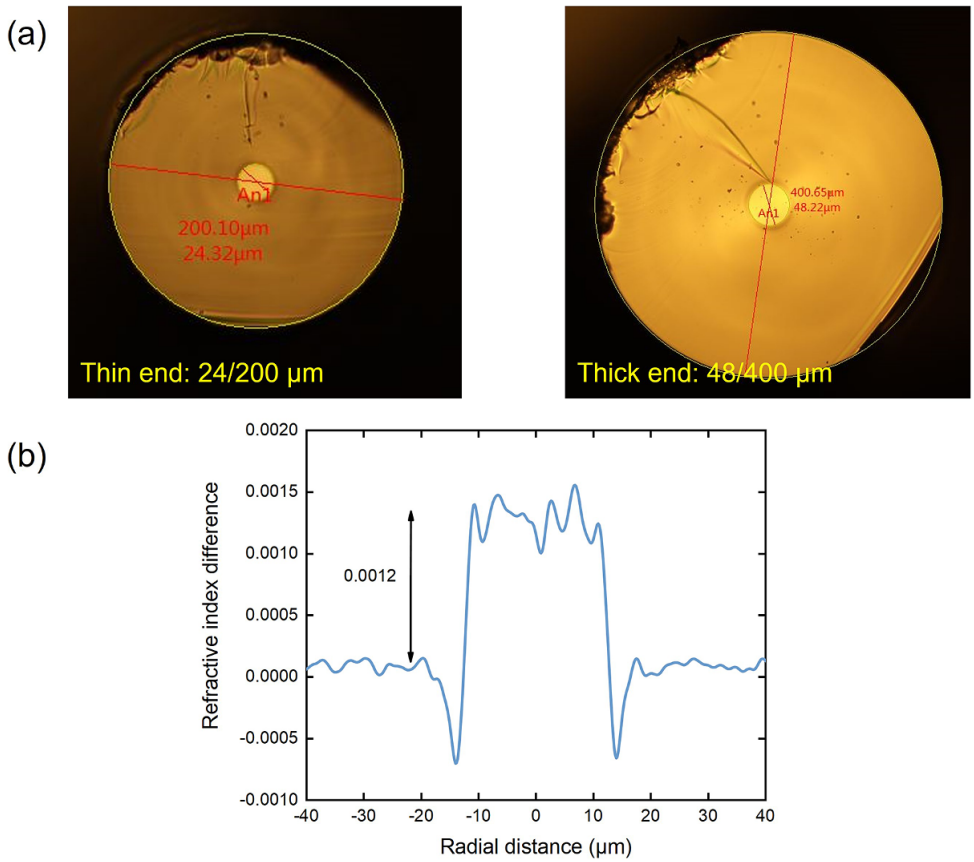

Figure 2. Geometric and refractive descriptions of the tapered fiber: (a) geometric dimensions at both ends; (b) measured refractive index profile.

3. Experimental results and simulations

The experimental setup for high-power delivery is shown in Figure 3(a), in which a monolithic fiber oscillator with an output power of over 1 kW and a 20/250 μm output fiber is employed as the laser source. This source operates at a signal wavelength of 1080 nm and has pure spectra at the whole power trace, that is, no SRS effect is observed. The 20/250 μm output fiber is optimally spliced with the thin end (i.e., 24/200 μm) of the tapered multimode fiber; the splicing optimization is taken from Ref. [36]. After splicing, the excited HOM contents in the whole delivery path are measured to be below –30 dB (the result will be presented in Figure 7), which ensures a high-fidelity delivery of the emitted laser beam from the 20/250 μm output fiber to the whole delivery path. To avoid unexpected mode coupling

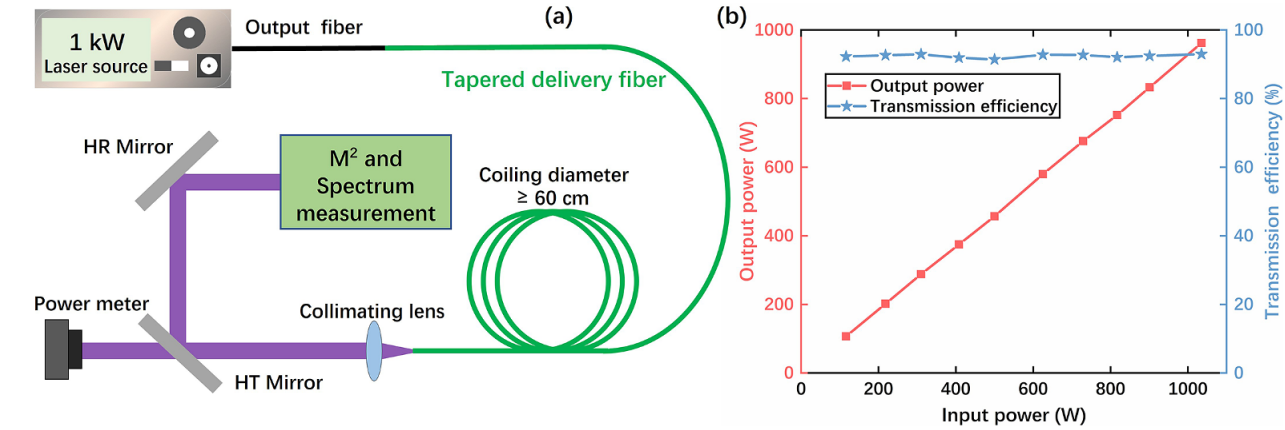

Figure 3. (a) Experimental setup for high-power delivery. (b) Relationship between the input and output power, and the total transmission efficiency.

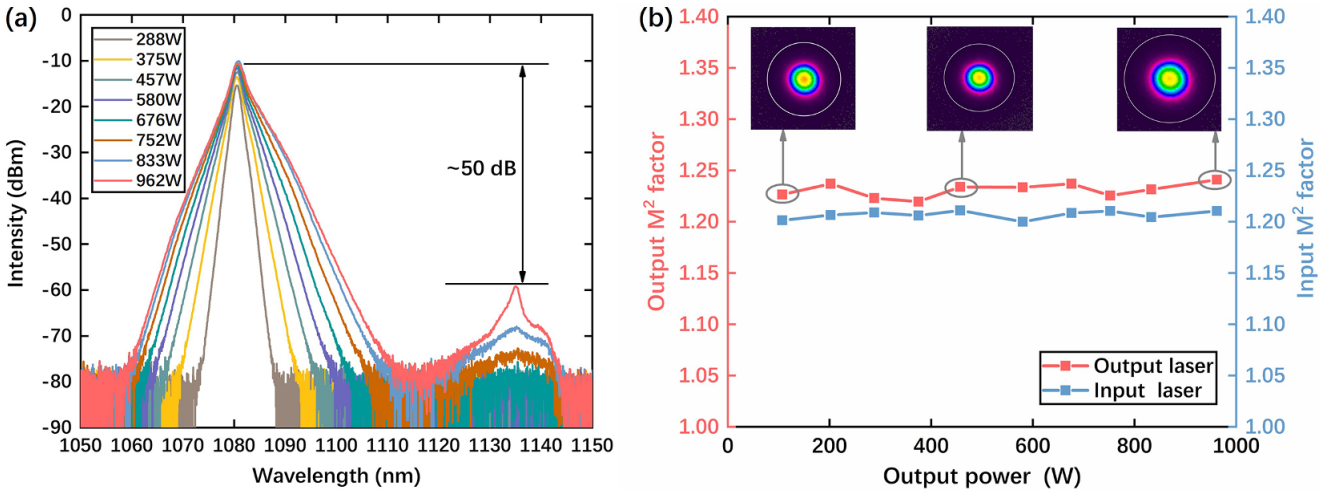

Figure 4. (a) Recorded spectra at different output powers. (b) Beam quality M^2 factors of the input and output laser.

induced by macro-bending, the tapered multimode fiber is loosely coiled with a 60 cm diameter. At the output end, a power meter, an optical spectrum analyzer and a beam quality analyzer are used for the laser beam characterization. The main power of the laser beam is transferred to the power meter through a high-transmittance (HT) mirror, and the sampled beam is directed by a high-reflectivity (HR) mirror. The trace of output power is plotted in Figure 3(b), which presents a linear correlation between the input and output power. The maximum output power is 962 W when the input laser is 1035 W. In the whole power trace, the transmission efficiency keeps a stable value of nearly 93%. This efficiency is mainly limited by the attenuation of the optical fiber, which could be further improved by increasing the NA.

The recorded spectra at different output powers are illustrated in Figure 4(a). At the highest output power, the signal-to-SRS ratio is over 50 dB, demonstrating the ideal suppression of the nonlinear effect after the whole delivery path of 105 m. To evaluate the mode fidelity after delivery, the beam quality M^2 factors of the input and output laser are recorded for comparison, as shown in Figure 4(b). The input M^2 factor represents the beam quality of the laser source emitted from the 20/250 μm output fiber. As can be seen, the input and output M^2 factors remain at stable values of nearly 1.20 and 1.23, respectively, indicating superior mode fidelity in the whole delivery path. The current results feature almost negligible beam quality degradation and demonstrate the excellent structure of the tapered fiber profile for mode preservation. The high-fidelity delivery reported here should be attributed to the following factors: (i) the optimum mode launching at the splicing point of the 20/250 μm output fiber and the thin end of the tapered fiber; (ii) the weakly coupled mechanism of the tapered multimode fiber by balancing the core diameter and NA; (iii) the excellent taper profile formed by fiber drawing.

The signal-to-SRS ratio for high-power delivery is determined by both the signal power and the initial Raman noise of the injected laser. In this experiment, although the laser source has an SRS-free spectrum at the highest power, the initial Raman noise is unknown. The SRS peak at the highest power in Figure 4(a) may be caused by high Raman noise at the input end. Note that spontaneous Raman noise varies

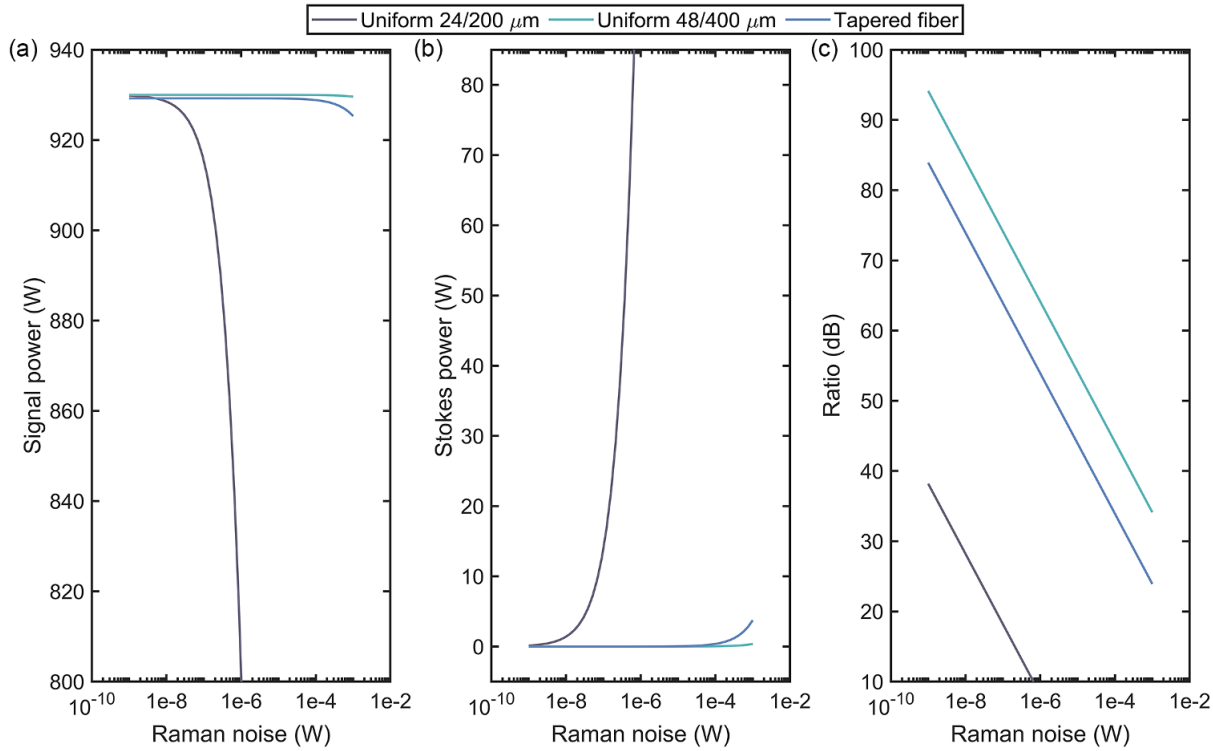

Figure 5. The evolutions of (a) signal and (b) Stokes power versus the injected Raman noise, and (c) the corresponding signal-to-SRS ratios in uniform fibers or the tapered fiber.

with the characteristics of different light sources; hence, the ultimate limit of high-power single-mode delivery should be considered dialectically. Since there is no effective method to detect the spontaneous Raman noise of the laser source at present, we try to explain the SRS dynamics in Figure 4(a) by further simulation. Three fiber configurations, namely the uniform 24/200 μm profile (105 m), the uniform 48/400 μm profile (105 m) and the tapered fiber profile (105 m, similar to the fiber used in this work) are considered. The NA of the three fibers is 0.06. The injected signal power is assumed to be 1000 W and the fiber attenuation is set to 3.5 dB/km.

Considering the Raman conversion in a long-distance delivery path, the power evolutions of the signal laser and Stokes light are highly correlated to the injected Raman noise. Due to the high-fidelity delivery of the single-mode laser in the experiment, it is reasonable to consider only the fundamental mode propagation. Then, the evolutions of the signal and Stokes power versus the injected Raman noise are expressed by the following[37]:

$$\begin{cases} \frac{dP_s}{dz} = -\frac{\lambda_r}{\lambda_s}\frac{g_R}{A_{eff}(z)}P_sP_r - \alpha_sP_s, \\ \frac{dP_r}{dz} = \frac{g_R}{A_{eff}(z)}P_rP_s - \alpha_rP_r, \end{cases} \tag{3}$$

where P_s and P_r represent the signal power and Stokes power, respectively, λ_s and λ_r represent the signal wavelength and Stokes wavelength, respectively, g_R is the Raman-gain coefficient, which is fixed to 6.43×10^{-14} W/m assuming that the polarization state is completely scrambled[38,39], α_s and α_r represent the background attenuation of the two wavelengths and $A_{eff}(z)$ is defined as the effective interaction area at different locations. In the tapered fiber, A_{eff} changes with the fiber length and could be written as Equation (4) at a specific location z:

$$\begin{aligned} A_{eff} &= \frac{\iint I_s dS \iint I_r dS}{\iint I_s I_r dS} \\ &= \frac{\int_0^{2\pi}\int_0^{r_{clad}}\left|\vec{E}_s(r,\varphi)\right|^2 r dr d\varphi \cdot \int_0^{2\pi}\int_0^{r_{clad}}\left|\vec{E}_r(r,\varphi)\right|^2 r dr d\varphi}{\int_0^{2\pi}\int_0^{r_{clad}}\left|\vec{E}_s(r,\varphi)\right|^2\left|\vec{E}_r(r,\varphi)\right|^2 r dr d\varphi}, \end{aligned} \tag{4}$$

where E and I represent the field and intensity distribution of the fiber eigenmode, respectively, and r and φ represent the radial and angular coordinates, respectively.

Based on Equations (3) and (4), the evolutions of signal and Stokes powers for the three fiber configurations are calculated for comparison, and the results are shown in Figure 5. We set a principle of 50 dB to evaluate the laser delivery performance, that is, a high-quality delivery is achieved if the final signal-to-SRS ratio is larger than 50 dB. It can be seen clearly in Figure 5(a) that, when the Raman noise changes from 1×10^{-9} to 1×10^{-6} W, the uniform 24/200 μm profile experiences a rapid decrement for the signal power due to the limited core mode area

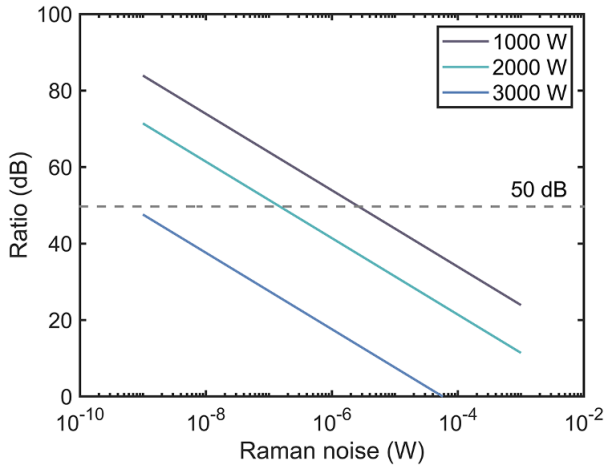

Figure 6. Evolution of signal-to-SRS ratios as a function of the injected Raman noise in the tapered multimode fiber with laser power levels of 1000, 2000 and 3000 W.

and a strong Raman conversion, accompanied by a sharp increase of Stokes power, as shown in Figure 5(b). In this case, the signal-to-SRS ratio degrades from 38 to 10 dB (when the Raman noise is nearly 1×10^{-6} W), as shown in Figure 5(c); hence, long-distance delivery cannot be accomplished through the uniform 24/200 μm fiber directly. As for the uniform 48/400 μm fiber, the signal and Stokes powers remain constant versus the varied Raman noise. Even with a larger Raman noise of 1×10^{-4} W, the signal-to-SRS ratio can reach nearly 50 dB, which enables high-quality delivery. For the tapered multimode fiber, the performance of high-power delivery is improved greatly compared with the uniform 24/200 μm fiber and shows results close to that of the uniform 48/400 μm fiber. This provides theoretical evidence of tapered multimode fiber for SRS-free delivery. Further, based on the experimental and simulated results, one can reasonably estimate that the laser source employed in the experiment has a spontaneous Raman noise of nearly 2×10^{-6} W.

The ultimate limits of the tapered multimode fiber for high-quality delivery are also investigated with different power levels. As illustrated in Figure 6, the signal-to-SRS ratio decreases over 12 dB when the laser power increases from 1000 to 2000 W. The principle (50 dB) of high-quality delivery restricts the injected Raman noise to 1.2×10^{-7} W. Hence, a laser source with a purer spectrum is needed to realize high-quality delivery at 2000 W by using the fiber drawn in this work. When the laser power is 3000 W, the signal-to-SRS ratio remains below 50 dB for the whole range. In this way, optimized design of the fiber profile, that is, the core dimensions, tapered length, etc., should be conducted to improve the performance.

The mode property is further characterized by using the spatially and spectrally resolved imaging technique[40] within the range of 1070–1090 nm, and the results are depicted in Figure 7. In the whole delivery path, five kinds of HOMs are weakly excited due to the intrinsic defects of the fiber structure. All of their peak-to-peak amplitudes are measured to be below –30 dB. Insets show the phase and intensity distributions of five HOMs, suggesting the typical patterns of the LP_{11}, LP_{21}, LP_{31}, LP_{12} and LP_{41} modes, respectively. No radial HOMs ($LP_{0,N}$ modes, where $N = 1, 2, 3, \ldots$) are observed in the whole path, which reveals the adiabatic property of the tapered region. The unexpected excitation of azimuthal HOMs is mainly attributed to the slight fluctuation of the fiber dimension since the actual fiber does not have theoretical uniformity. The mode preservation ensures the immunity of the delivery system for preventing beam quality degradation over a long distance.

With a weakly coupled regime, the current results of the M^2 factor and mode diagnosis demonstrate the convenience of high-fidelity delivery. To achieve this goal, a key premise is controlling the launching condition. Once the laser modes are coupled into the delivery fiber with high fidelity, the weakly coupled regime can keep the field contents intact.

4. Discussion: ultimate limits for high-power, single-mode and long-distance delivery based on solid-core fibers

As high-power laser delivery becomes a reawakened subject, many power records have been generated for long-distance and single-mode transmission in recent years. To pursue the bilateral limits for power and delivery length, the transmission characteristics with different presupposed parameters should be further discussed. Considering the difference of laser sources in terms of Raman noise, it is not meaningful to estimate the SRS threshold directly by the simplified formula $P_{\mathrm{th}} \approx 16A_{\mathrm{eff}}/(g_{\mathrm{R}}\cdot L)$, in which A_{eff}, g_{R} and L represent the effective mode area, Raman-gain coefficient and fiber length, respectively. The final signal-to-Stokes ratio is affected by the laser power, Raman noise, fiber parameters and delivery length synchronously.

Based on the weakly coupled condition and the fiber parameters used in this work, the further discussion here assumes the core diameter to be 48 μm, and the NA is 0.06. For simplicity and universality, the uniform fiber profile is selected for reference. The transmission attenuation at 1080 nm is set to 5 dB/km. This is a moderate value of attenuation for current passive laser fibers. In all the simulations, an ideal single-mode beam is adopted, since the experiment described in this work has verified the inherent advantage of a tapered fiber scheme for high-fidelity delivery, and this technique can be widely extended. The simulations also obey the power evolution in Equation (3).

Figure 8 displays the relationships between the initial Raman noise and the output properties with different fiber lengths and an injected signal power of 1000 W. For the delivery length of 100 m, the output signal power keeps a

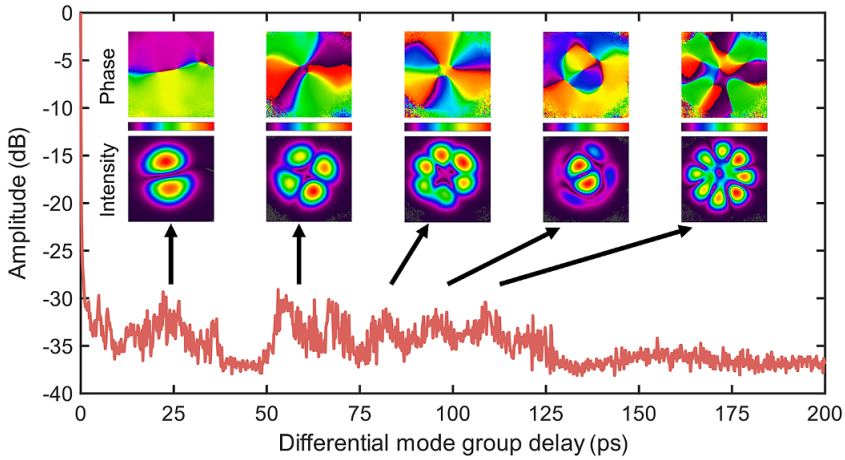

Figure 7. Spatially and spectrally resolved imaging results for the whole delivery path.

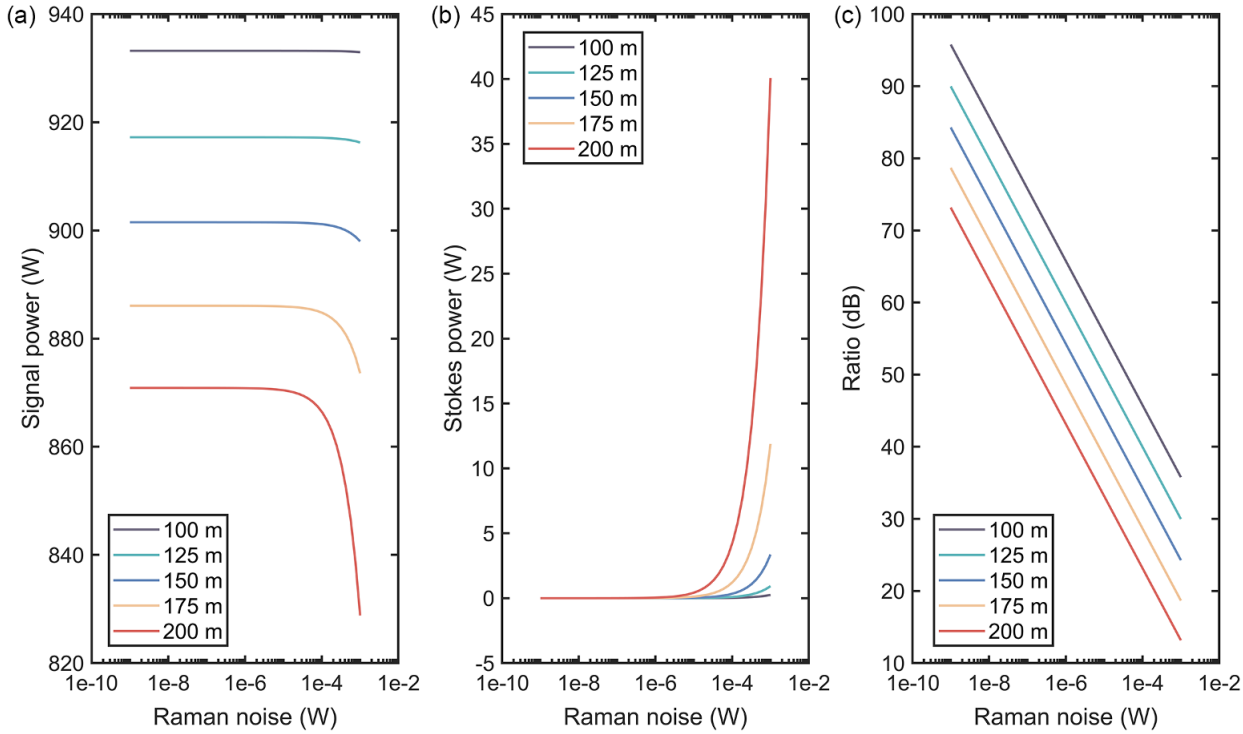

Figure 8. Relationships between the initial Raman noise and the output properties with different fiber lengths and an injected signal power of 1000 W: (a) output signal power; (b) output Stokes power; (c) output signal-to-Stokes ratio.

stable value of nearly 935 W. Even with a large Raman noise, for example, 1×10^{-3} W, the Stokes power does not increase significantly, and the signal-to-Stokes ratio is estimated to be higher than 35 dB. If we set a signal-to-Stokes ratio of 50 dB as the principle for high-quality delivery, the initial Raman noise power of the laser source should be maintained of the order of 10^{-4} W or lower when the delivery length is 100 m. As the delivery length extends to 150 m, a stronger Raman conversion is observed. At the maximum Raman noise, the conversion of signal light and Stokes light experiences a significant increment, resulting in a signal-to-Stokes ratio of less than –30 dB at the output end. According to the calculation results, it is a challenging task to obtain a high-quality delivery of 175 or 200 m for a 1000 W single-mode laser. To achieve these goals, the Raman noises of the laser source should be controlled to below the orders of 1×10^{-6} and 1×10^{-7} W, respectively.

Similarly, Figure 9 displays the relationships between the initial Raman noise and the output properties with different fiber lengths and an injected signal power of 2000 W. When the delivery length is 50 m, the signal-to-Stokes ratio remains over 40 dB if the Raman noise varies from 1×10^{-9} and 1×10^{-3} W. To realize a signal-to-Stokes ratio over 50 dB, the power level of the Raman noise should be less than the

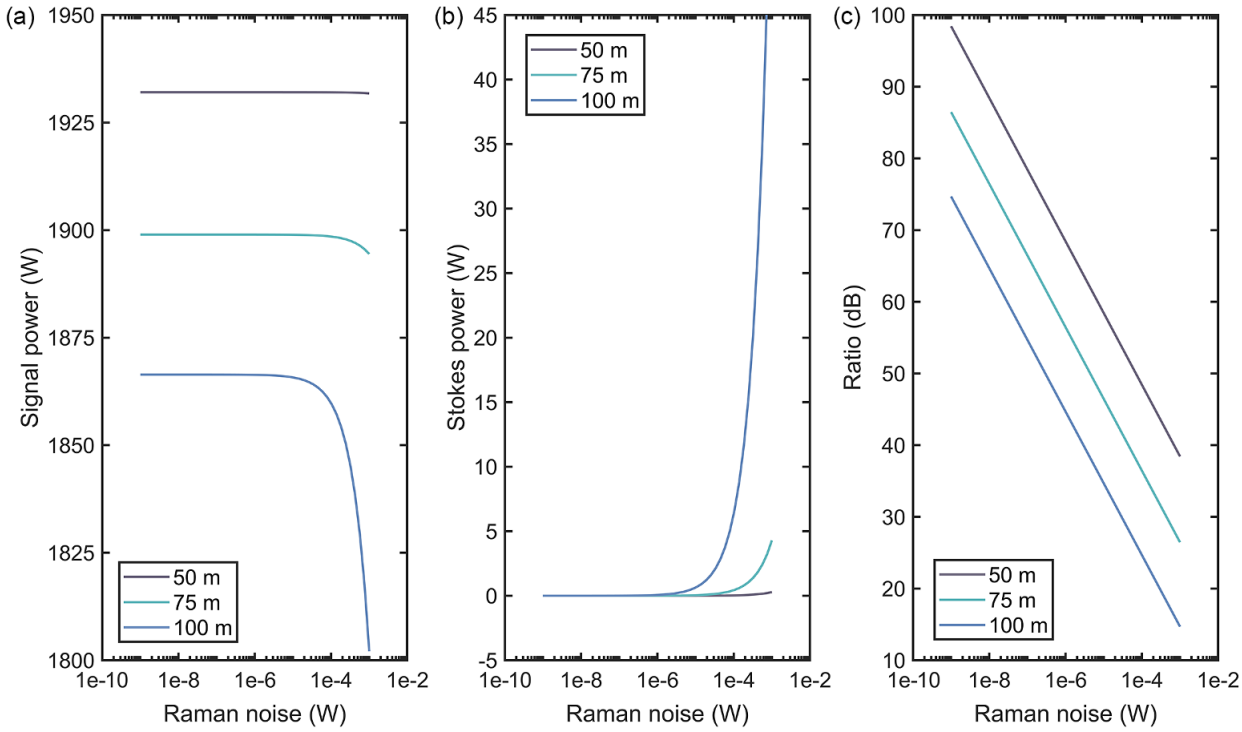

Figure 9. Relationships between the initial Raman noise and the output properties with different fiber lengths and an injected signal power of 2000 W: (a) output signal power; (b) output Stokes power; (c) output signal-to-Stokes ratio.

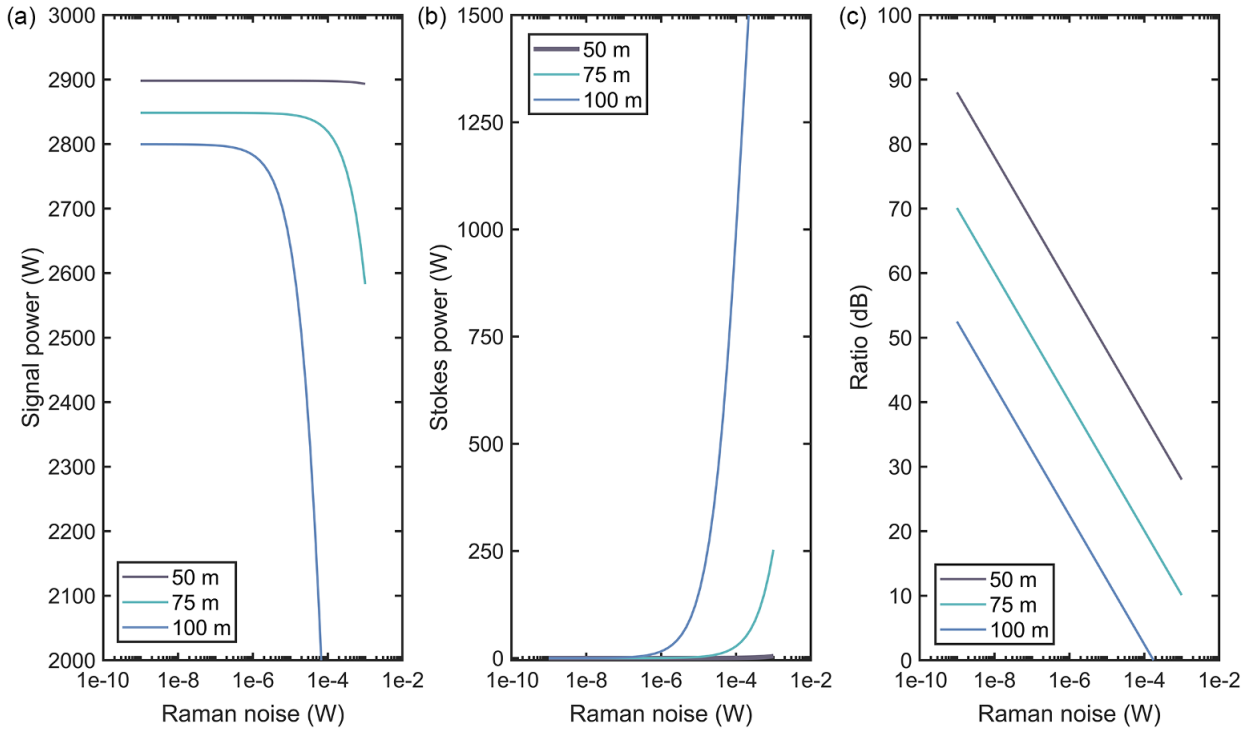

Figure 10. Relationships between the initial Raman noise and the output properties with different fiber lengths and an injected signal power of 3000 W: (a) output signal power; (b) output Stokes power; (c) output signal-to-Stokes ratio.

order of 1×10^{-4} W, meaning that the 2 kW laser source should have an initial signal-to-SRS ratio larger than 73 dB. Consequently, the demand for high-power, single-mode laser delivery puts forward higher requirements on developing laser sources with high spectral purity. When the delivery length is 75 m, high-quality delivery restricts the Raman

noise to nearly the order of 1×10^{-5} W; in this case, the initial signal-to-SRS ratio of the laser source is over 83 dB. When the delivery length is 100 m, an obvious Raman conversion can be seen if the Raman noise is larger than 1×10^{-6} W, which degrades the transmission efficiency and spectral purity. In other words, based on solid-core fibers of below 50 μm, it is a tough target to achieve a delivery length of over 100 m at the power level of 2000 W.

To determine the ultimate limits of high-power delivery, the cases for 3000 W are also calculated, as shown in Figures 10(a)–10(c). When the Raman noise is 1×10^{-4} W, the signal-to-Stokes ratios for 50, 75 and 100 m delivery lengths are 38, 20 and 2.3 dB, respectively. When the Raman noise is 1×10^{-5} W, the signal-to-Stokes ratios for 50, 75 and 100 m delivery lengths are 48, 30 and 12 dB, respectively. When the Raman noise is 1×10^{-6} W, the signal-to-Stokes ratios for 50, 75 and 100 m delivery lengths are 57, 39 and 22 dB, respectively. When the Raman noise is 1×10^{-7} W, the signal-to-Stokes ratios for 50, 75 and 100 m delivery lengths are 68, 50 and 32 dB, respectively. As for the delivery length of 100 m, the requirement on Raman noise is lower than 1×10^{-9} W if a signal-to-Stokes ratio of over 50 dB is expected.

5. Conclusion

The current work provides a successful scheme to balance the nonlinear effects and beam quality degradation for the long-distance delivery of high-power single-mode lasers. Here, we experimentally realize a kilowatt-level delivery of 105 m enabled by a tapered multimode fiber. With the maximum input power of 1035 W, the maximum output power is 962 W, corresponding to a high efficiency of over 93% and a high signal-to-SRS ratio of over 50 dB. The tapered multimode fiber is carefully designed with the weakly coupled condition and adiabatically drawn from a thin end of 24/200 μm to a thick end of 48/400 μm. Due to the excellent taper profile and the optimum excitation at the input end, high-fidelity delivery without beam deterioration is demonstrated, which results in M^2 factors of 1.20 and 1.23 for the input and output lasers, respectively. The mode property resolved by the mode imaging technique shows slight HOM contents of less than –30 dB in the whole delivery path, which further supports the evidence of high-fidelity transmission.

To observe the ultimate limits for high-power laser delivery, the output properties of 48 μm fibers with different delivery lengths and laser powers are calculated as a function of the injected Raman noise. We set a high signal-to-Stokes ratio of 50 dB to evaluate high-quality delivery. Results show that, for solid-core fibers below 50 μm, it is a challenging task to obtain high-quality delivery of 175 or 200 m for a 1000 W single-mode laser unless the Raman noises of the laser source are controlled to below the orders of 1×10^{-6} or 1×10^{-7} W, respectively. Similarly, a delivery length of over 100 m at the power level of 2000 W restricts the Raman noise to be lower than the order of 1×10^{-6} W. When the laser power is 3000 W, the different orders of Raman noise, that is, 1×10^{-6}, 1×10^{-7} and 1×10^{-9} W, determine the ultimate delivery lengths to be 50, 75 and 100 m, respectively.

In addition, the scheme of tapered delivery fiber can be easily combined with functional schemes. Since the tapered fiber modulates the light transmission along the longitudinal direction, it is a promising method to incorporate it with transverse designs, including designs with stronger HOM suppression, weaker light–acoustics interaction, etc.

Acknowledgements

This work was supported by the National Key R&D Program of China (No. 2022YFB3606000) and the Graduate Innovation Project of Hunan Province (No. QL20220004).

References

1. H. C. H. Mulvad, S. Abokhamis Mousavi, V. Zuba, L. Xu, H. Sakr, T. D. Bradley, J. R. Hayes, G. T. Jasion, E. Numkam Fokoua, A. Taranta, S. U. Alam, D. J. Richardson, and F. Poletti, Nat. Photonics **16**, 448 (2022).
2. J. Yao, X. Zhang, B. Li, B. Wang, D. Jin, Y. Duan, J. Zhao, and P. Wang, J. Lightwave Technol. **42**, 5710 (2024).
3. M. A. Cooper, J. Wahlen, S. Yerolatsitis, D. Cruz-Delgado, D. Parra, B. Tanner, P. Ahmadi, O. Jones, M. S. Habib, I. Divliansky, J. E. Antonio-Lopez, A. Schülzgen, and R. Amezcua Correa, Optica **10**, 1253 (2023).
4. C. Rohrer, C. A. Codemard, G. Kleem, T. Graf, and M. A. Ahmed, J. Lightwave Technol. **37**, 4260 (2019).
5. C. N. Danson, C. Haefner, J. Bromage, T. Butcher, J.-C. F. Chanteloup, E. A. Chowdhury, A. Galvanauskas, L. A. Gizzi, J. Hein, D. I. Hillier, N. W. Hopps, Y. Kato, E. A. Khazanov, R. Kodama, G. Korn, R. Li, Y. Li, J. Limpert, J. Ma, C. H. Nam, D. Neely, D. Papadopoulos, R. R. Penman, L. Qian, J. J. Rocca, A. A. Shaykin, C. W. Siders, C. Spindloe, S. Szatmári, R. M. G. M. Trines, J. Zhu, P. Zhu, and J. D. Zuegel, High Power Laser Sci. Eng. **7**, e54 (2019).
6. J. Zuo and X. Lin, Laser Photonics Rev. **16**, 2100741 (2022).
7. W. Shi, Q. Fang, X. S. Zhu, R. A. Norwood, and N. Peyghambarian, Appl. Opt. **53**, 6554 (2014).
8. C. Jauregui, J. Limpert, and A. Tünnermann, Nat. Photonics **7**, 861 (2013).
9. M. O'Connor, V. Gapontsev, V. Fomin, M. Abramov, and A. Ferin, in *Conference on Lasers and Electro-Optics/International Quantum Electronics Conference*, OSA Technical Digest (CD) (Optica Publishing Group, 2009), paper CThA3.
10. S. Kensuke, I. Shinya, U. Keisuke, T. Yuya, K. Masahiro, and T. Daiichiro, Proc. SPIE **10512**, 105120C (2018).
11. X. Chen, T. Yao, L. Huang, Y. An, H. Wu, Z. Pan, and P. Zhou, Adv. Fiber Mater. **5**, 59 (2023).
12. H. Wu, X. Chen, L. Huang, and P. Zhou, in *Specialty Optical Fibers*, M. F. S. Ferreira and M. C. Paul, eds. (Elsevier, 2024), pp. 207–230.
13. X. Zhang, S. F. Gao, Y. Y. Wang, W. Ding, and P. Wang, High Power Laser Sci. Eng. **9**, e23 (2021).
14. D. Jain, Y. Jung, M. Nunez-Velazquez, and J. K. Sahu, Opt. Express **22**, 31078 (2014).

15. Y. An, H. Yang, X. Chen, L. Huang, Z. Yan, Z. Pan, Z. Wang, Z. Jiang, and P. Zhou, Opt. Lett. **48**, 61 (2023).
16. S. Hochheim, E. Brockmüller, P. Wessels, M. Steinke, J. Koponen, T. Lowder, S. Novotny, J. Neumann, and D. Kracht, J. Lightwave Technol. **39**, 7246 (2021).
17. X. Chen, L. Huang, H. Yang, X. Xi, Y. An, Z. Yan, Y. Chen, Z. Pan, and P. Zhou, Opt. Laser Technol. **157**, 108668 (2023).
18. H. Li, C. Goel, J. Zang, S. Raghuraman, S. Chen, M. R. Abu Hassan, W. Chang, and S. Yoo, Opt. Express **30**, 7928 (2022).
19. T. Matsui, K. Tsujikawa, T. Okuda, N. Hanzawa, Y. Sagae, K. Nakajima, Y. Fujiya, and K. Shiraki, IEICE Trans. Commun. **E103.B**, 415 (2020).
20. X. Zhu, D. Wu, Y. Wang, F. Yu, Q. Li, Y. Qi, J. Knight, S. Chen, and L. Hu, Opt. Express **29**, 1492 (2021).
21. D. Wu, F. Yu, C. Wu, M. Zhao, J. Zheng, L. Hu, and J. Knight, Opt. Express **31**, 21870 (2023).
22. H. Sakr, Y. Chen, G. T. Jasion, T. D. Bradley, J. R. Hayes, H. C. H. Mulvad, I. A. Davidson, E. Numkam Fokoua, and F. Poletti, Nat. Commun. **11**, 6030 (2020).
23. S. Gao, Y. Wang, W. Ding, D. Jiang, S. Gu, X. Zhang, and P. Wang, Nat. Commun. **9**, 2828 (2018).
24. Q. Fu, Y. Wu, I. A. Davidson, L. Xu, G. T. Jasion, S. Liang, S. Rikimi, F. Poletti, N. V. Wheeler, and D. J. Richardson, Opt. Lett. **47**, 5301 (2022).
25. Q. Fu, I. A. Davidson, S. M. A. Mousavi, H. C. H. Mulvad, N. V. Wheeler, L. Xu, F. Poletti, and D. J. Richardson, Laser Photonics Rev. **18**, 2201027 (2024).
26. S. Jiang, L. Ma, Z. Zhang, X. Xu, S. Wang, J. Du, C. Yang, W. Tong, and Z. He, J. Lightwave Technol. **36**, 5547 (2018).
27. M. Fermann, Opt. Lett. **23**, 52 (1998).
28. S. Hurand, L.-A. Chauny, H. El-Rabii, S. Joshi, and A. Yalin, Appl. Opt. **50**, 492 (2011).
29. A. P. Yalin, Opt. Express **21**, A1102 (2013).
30. L. Bansal, R. Sienkowski, C. Neale, J. Mann, and J. W. Nicholson, Proc. SPIE **12866**, 1286604 (2024).
31. X. Chen, S. Huang, L. Huang, L. Du, Z. Yan, Z. Pan, P. Zhou, and Z. Jiang, High Power Laser Sci. Eng. **12**, e54 (2024).
32. D. Marcuse, *Theory of Dielectric Optical Waveguides*, 2nd Edition (Academic Press, 1991), pp. 60–96.
33. J. M. Fini, Opt. Lett. **32**, 1632 (2007).
34. J. M. Fini and S. Ramachandran, Opt. Lett. **32**, 748 (2007).
35. M.-J. Li, X. Chen, A. Liu, S. Gray, J. Wang, D. T. Walton, and L. A. Zenteno, J. Lightwave Technol. **27**, 3010 (2009).
36. V. Scarnera, C. A. Codemard, M. Durkin, and M. N. Zervas, Proc. SPIE **12865**, 1286515 (2024).
37. J. Ji, C. A. Codemard, M. Ibsen, J. K. Sahu, and J. Nilsson, IEEE J. Sel. Top. Quantum Electron. **15**, 129 (2009).
38. G. P. Agrawal, in *Nonlinear Science at the Dawn of the 21st Century* (Springer, 2000), pp. 195–211.
39. S. T. Davey, D. L. Williams, B. J. Ainslie, W. J. M. Rothwell, and B. Wakefield, IEE Proc. J. **136**, 301 (1989).
40. J. W. Nicholson, A. D. Yablon, J. M. Fini, and M. D. Mermelstein, IEEE J. Sel. Top. Quantum Electron. **15**, 61 (2009).